Elementary electronic excitations in one-dimensional continuum and lattice systems

D. W. Wang and S. Das Sarma
Department of Physics, University of Maryland, College Park, Maryland 20742-4111
(Received 8 January 2001; revised manuscript received 20 June 2001; published 13 December 2001)

We systematically investigate the mode dispersion and spectral weight of the elementary excitation spectra in one-dimensional continuum and lattice electron systems by using the RPA, the Luttinger liquid model, and the Hubbard model. Both charge and spin excitations are studied in detail and compared among the theoretical models. For the lattice Hubbard model we use both Bethe-ansatz equations and Lanczos-Gagliano method to calculate dispersion and spectral weight separately. We discuss the theoretically calculated elementary excitation spectra in terms of the experimental inelastic light (Raman) scattering spectroscopy of one-dimensional (1D) semiconductor quantum wire systems. Our results show that in the polarized (i.e., non-spin-flip) Raman-scattering spectroscopy, only the 1D charge density excitations should show up with observable spectral weight with the single-particle excitations (in random-phase approximation) or singlet spin excitations (in the Luttinger model and the Hubbard model) having negligible spectral weight. The depolarized (spin-flip) Raman-scattering spectra manifest the spin density or the triplet spin excitations. We also provide a qualitative comparison between the continuum and the lattice 1D elementary excitation spectra.

DOI: 10.1103/PhysRevB.65.035103 PACS number(s): 71.10.Fd, 71.15.−m, 78.30.Fs, 78.35.+c

I. INTRODUCTION

The goal of this paper is to investigate theoretically the charge and spin elementary excitation spectra as well as their spectral weights in one-dimensional (1D) electron systems,[1–3] both for a continuum jellium electron gas and for an atomic lattice model. Our calculations (in particular, our spectral weight calculations) should apply to the experimental Raman-scattering data[4–6] if the resonance effects are dynamically unimportant in the interpretation of the Raman experiments. We refer to our calculations as the nonresonant Raman scattering (NRS) theory where only the conduction-band electrons are taken into account as opposed to the resonant Raman scattering where both the conduction band and the valence band participate. In fact, the theory developed in this paper has been the standard theory for discussing the resonant Raman-scattering spectroscopy until very recently when several publications[7–9] dealing with the full subtleties of the resonance effect have appeared in the literature. We emphasize that, quite apart from the resonant Raman-scattering spectroscopy, theoretical results presented in this paper stand on its own as a comprehensive theory for the elementary excitation spectra of 1D electron systems.

In this paper, we will study the standard (nonresonant) Raman-scattering spectroscopy in three theoretical models: the random-phase-approximation (RPA) Fermi-liquid model, the Luttinger liquid (LL) model, and the 1D Hubbard model. As emphasized above, by ''nonresonant'' we mean that the theory neglects all effects of the valence band in resonant Raman scattering (which is a two-step process, with the incident photon being absorbed by a valence-band electron which thereby gets excited into an excited conduction-band state with an electron from inside the conduction-band Fermi surface subsequently combining with the valence-band hole with the emission of the scattered photon). If the valence band can be ignored, then only conduction-band density fluctuations are responsible in the linear response theory of the scattering process. The calculation is then simplified to the evaluation of the density-density correlation function (for polarized spectrum) and the spin-density correlation function (for depolarized spectrum), whose imaginary parts are proportional to the spectra measured in the experiments. This approach of identifying the measured elementary excitation spectra in the Raman-scattering experiments as the charge (polarized spectra) or the spin- (depolarized) density correlation function of the electron system in the conduction band has a long and fairly successful history[10] in the semiconductor structures. We take the same approach here, and construct our charge and spin-density correlation functions (which give the spectral strengths of the elementary excitations through their imaginary parts or the corresponding dynamical structure factors) entirely from the conduction-band carriers, ignoring all effects of the valence band in the resonance process.

There has been one persistent feature in the experimental Raman spectra of semiconductor systems, including 1D QWR structures, which does not seem to have an obvious explanation in terms of the nonresonant theory discussed in this paper. There is often a low-energy spectral peak in the polarized spectra at an energy well below the expected collective charge-density excitation (CDE) peak (and in addition to the charge-density excitation peak, which always shows up at the usual energy). This additional peak occurs around the single-particle excitation energy, which typically contributes little to the dynamical structure factor (i.e., the density correlation function) at the low wave vectors ($q \ll k_F$) of Raman-scattering experiment, and therefore should have negligible (unobservable) spectral weight. There have been many suggestions for the resolution of this puzzle (namely, why the single-particle excitation weight is enhanced in the density correlation spectrum), and we will quantitatively consider several of these suggestions in this paper. Our conclusion, based on the results presented in this paper, is that this puzzle in all likelihood arises necessarily from the resonant nature of Raman-scattering experiments, as has recently been argued in the literature,[7–9] which is be-

yond the scope of this paper. Our critical quantitative consideration of the several suggested scenarios (within the nonresonant theory of using conduction-band properties only) for explaining why the single-particle excitation has large spectral weight shows that none of them is capable of resolving this problem quantitatively. While studying the 1D elementary excitation spectra is the primary goal of this paper, considering the single-particle excitation spectral weight issue in the nonresonant Raman scattering is one of our important secondary goals.

We first present the results of the Fermi-liquid random-phase-approximation (RPA) calculation for this problem in Sec. II. The RPA calculation has been shown to give a good description[11] for the dispersion relations of the elementary excitations in comparison with the experimental results,[4] for both intersubband and intrasubband 1D excitations.[12] Being a standard Fermi liquid (FL) theory, however, the RPA calculation is unable to explain the relatively large spectral weight of the ''single-particle excitation'' (SPE) in the polarized spectrum of the experiment as discussed above. We include the effects of the breakdown of momentum conservation and the nonparabolic energy dispersion in our calculation to check if they can explain the SPE feature within RPA, but neither gives qualitatively correct results for the polarized spectrum. In the Luttinger liquid model we present in Sec. III, we find *zero* weight at the SPE energy (as we should, since in the LL model there are no single-particle-like quasiparticle excitations), and all the spectral strength is at the charge boson mode, which is exactly the CDE mode in RPA. In Sec. IV, we use the 1D (lattice) Hubbard model with repulsive on-site spin-dependent interaction to study this problem. The study of 1D elementary excitations and the associated spectral weights in the Hubbard model is one of our main results in this paper. This Hubbard model study was originally motivated by the suggestion in Ref. 13 that a possible way to interpret this SPE puzzle (the existence of a single-particle peak in Raman scattering) in 1D should be different from those in higher dimensions, and the so-called SPE peak may be arising from the spin-singlet excitations (SSE) of interacting 1D systems.[13,14] Therefore we choose to study in detail the 1D Hubbard model, in which the spin-dependent interaction is expected to enhance the contribution of the spin-singlet excitation, which is proposed[13,14] as the extra SPE-like feature showing up in the experiment. Although the Hubbard model is a lattice model and consequently may not apply directly to the continuum QWR system, we argue that it is useful to understand the detailed excitation spectra in the 1D Hubbard model in the context of this problem because one can quantitatively study the interacting 1D elementary excitation spectra using the Hubbard model.

II. FERMI-LIQUID MODEL

The Fermi-liquid calculation of the elementary excitation spectrum of an electron system has been extensively discussed in the literature.[3,10–12,15,16] We use two standard approximations: RPA and the Hubbard approximation.[15–17] We refer the reader to the existing literature[3,10–12,15–17] for details

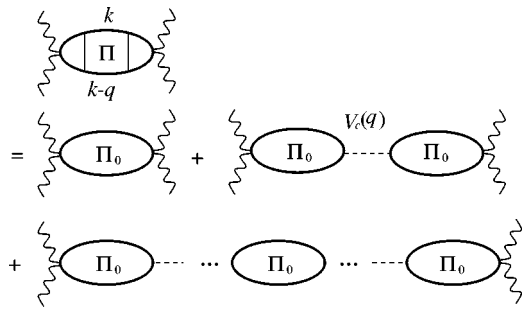

FIG. 1. Diagrammatic representation of the conduction-band irreducible polarizability $\Pi_0(q,\omega)$ and reducible polarizability $\Pi(q,\omega)$ in standard RPA calculation. $V_c(q)$ is the Coulomb interaction.

on RPA and the Hubbard approximation (HA) except to note here that in RPA one uses the noninteracting electron polarizability function (Fig. 1) for the irreducible response function and in the HA one includes an approximate local-field correction $G(q)$ to crudely incorporate the exchange vertex correlations. We use the following simple form for the 1D Hubbard local-field correction:

$$G(q)=\frac{1}{2}\frac{V_c(\sqrt{q^2+k_F^2})}{V_c(q)}, \tag{1}$$

where $V_c(q)$ is the 1D Coulomb interaction and k_F is the 1D Fermi wave vector. In the long-wavelength limit, $q\to 0$, $G(q)\to 0$ for Coulomb interaction and the RPA result is restored in the long-wavelength limit as it must. In Fig. 2 we plot the dispersion and spectrum of the 1D charge density collective excitation (usually called the 1D plasmon mode) within both the RPA and the Hubbard approximation—the plasmon mode is defined by the zero of the dielectric function and the intensity or the spectral weight is given by the imaginary part of the dielectric function (i.e., the dynamical structure factor[15]). In Fig. 2(a), we find that the plasmon energy is actually larger than the SPE continuum energy for all momentum, so that there is no Landau damping in the 1D system within the RPA calculation. The 1D plasma dispersion has no gap in the long-wavelength limit, but an infinite slope at $q=0$ due to the logarithmic divergence of the 1D Coulomb interaction.

In Fig. 2(b), we also show the typical calculated polarized RRS spectrum using a phenomenological broadening factor, $\gamma=0.05E_F$, which may be arising from impurity scattering. We find that the spectral weight of CDE is much larger than that of SPE (about one thousand times!). In the same figure we show the HA results as well. We find that while the vertex correction indeed increases the SPE weight somewhat relative to the CDE weight, the HA is still completely unable (by a factor of 100) to explain the experimental finding[4] of the SPE mode being comparable in the intensity to the CDE mode (double peak structure) in the polarized RRS spectrum.[4] Moreover, if the electron energy dispersion is linear (as it is close to the Fermi point), the SPE excitation spectral weight disappears. This indicates that the band curvature around k_F plays an important role in forming the SPE peak in the experiments. For example, in the linearized LL

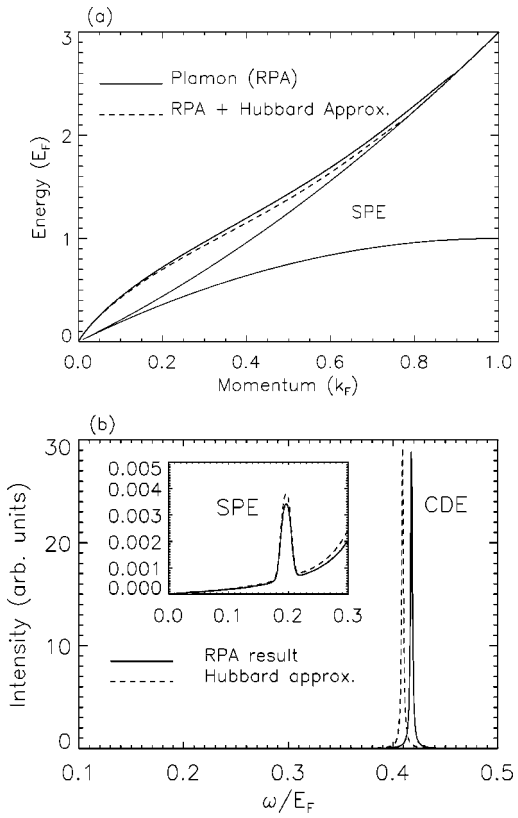

FIG. 2. (a) The energy-momentum dispersion relation for the plasmon mode and the SPE region of 1D system. (b) The dynamical structure factor of the polarized RRS spectrum in RPA calculation for the 1D quantum wire system at $q=0.1k_F$. Vertex correction in Hubbard approximation is also shown for comparison. Parameters are the same as the experiments in Ref. 4. Finite broadening factor is involved to present the delta-function peaks.

theory the SPE will have exactly zero spectral weight. Below we consider the band nonparabolicity effect explicitly.

In discussing the spin-desity excitation (SDE) spectrum in the depolarized goemetry we note that the depolarized spectrum of 1D electron systems in the RPA is just the imaginary part of the noninteracting polarizability function ($\mathrm{Im}\Pi_0$) which is the same as the SPE in the polarized spectrum. Thus within RPA the depolarized mode dispersion is identical to the SPE energy, i.e., $\omega=qv_F$ with a q^2 broadening. One should note, however, that when vertex corrections such as in the Hubbard approximation are taken into account, the spectra of the SDE will not be exactly the same as the SPE due to the vertex correction induced energy shift. In Fig. 3 we show the SDE spectrum obtained by calculating the spin-density correlation function in RPA and also in the Hubbard approximation. The vertex correction shifts the SDE peak to lower energy (an excitonic shift) in the HA and thus separates it from the SPE mode.

Beyond the standard RPA calculation, we include two nongeneric effects, the breakdown of momentum conservation (arising from impurity scattering, for example) and the nonparabolicity of electron energy dispersion, because both of these corrections are likely to transfer some large wave-vector SPE weight to smaller wave vector. For the breakdown of momentum conservation, we use a phenomenological approach[18] by introducing a broadening function that couples the polarized spectrum $\chi_\rho(q,\omega)$ at momentum q to that at momentum q':

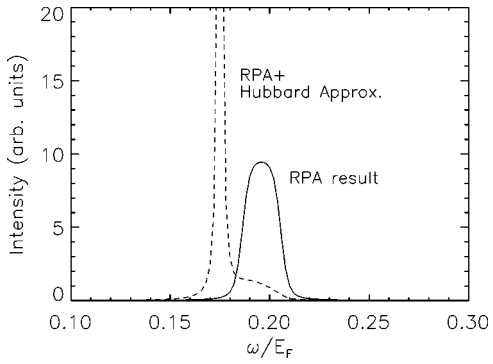

FIG. 3. The dynamical structure factor of the depolarized RRS spectrum calculated from $\mathrm{Im}\Pi^{\mathrm{RPA}}_{0,\sigma}(q,\omega)$ within RPA and Hubbard approximation.

$$\chi_\rho(q,\omega;\Gamma)\sim\frac{\Gamma k_F}{\pi}\int dq'\frac{\chi_\rho(q',\omega)}{(q-q')^2+\Gamma^2k_F^2}, \tag{2}$$

where Γ is a (phenomenological) dimensionless factor denoting the strength of the breakdown of momentum conservation. For $\Gamma\to0$ we get back the original spectrum. In Fig. 4(a), we show the numerical calculation results of this effect by applying Eq. (2) onto the RPA result. At first sight, one finds that finite Γ does decrease the peak value of CDE and enhance the SPE weight. For $\Gamma>0.5$, however, we find that the SPE peak merges into the very broad CDE peak, which is broadened also by the breakdown of momentum conservation. In other words, the breakdown of momentum conservation reduces the CDE peak strength and also broadens its width without changing either the total CDE spectral weight or the SPE weight qualitatively. Therefore, in our direct numerical calculation, we show that the breakdown of momentum conservation is not the candidate mechanism to provide an SPE spectral weight comparable to the CDE weight in RPA calculations.

We now discuss the same issue by considering the band nonparabolicity effect of the electron energy dispersion. We recalculate the RPA spectral weight including band nonparabolicity via an additional q^4 term in the electron energy dispersion,[19]

$$\frac{E(q;\lambda)}{E_F}=\left(\frac{q}{k_F}\right)^2+\lambda\left[\left(\frac{q}{k_F}\right)^4-\left(\frac{q}{k_F}\right)^2\right]. \tag{3}$$

This expression of $E(q;\lambda)$ keeps the Fermi energy constant $[E(k_F;\lambda)=E_F]$ for all λ and changes the electron effective mass $m_e(\lambda)=m/(1-\lambda)$ consistently. In Fig. 4(b), we show the calculated polarized RRS spectrum for different values of $\lambda\leqslant0.1$. We find that the enhancement of the SPE weight is very small, while the CDE peak almost keeps the same weight. Using larger λ will cause greater blue shifts in both SPE and CDE energies due to the increase of Fermi velocity,

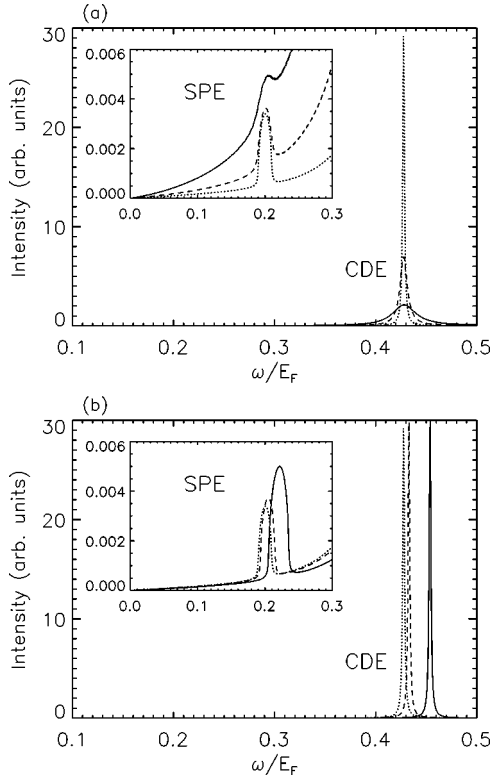

FIG. 4. The dynamical structure factor of the polarized RRS spectrum calculated by including (a) the breakdown of momentum conservation and (b) the nonparabolic energy dispersion. The dot, dashed, and solid lines in (a) represent the broadening parameter $\Gamma=0$, 10^{-3}, and 4×10^{-3}, respectively [see Eq. (2)], and in (b) represent the nonparabolicity parameter $\lambda=0$, 0.02, and 0.1, respectively [see Eq. (3)]. All these effects cannot enhance the SPE spectral weight to be comparable to CDE in the reasonable range of Γ or λ.

which disagrees with the experimental results (note that the standard RPA results provide very good agreement with the experimental results in the excitation energies[4]). Therefore the nonparabolicity effect cannot enhance the SPE spectral weight to be comparable to the CDE weight.

III. LUTTINGER LIQUID MODEL

The Luttinger liquid model[1,2,14] is thought to provide a generic low-energy description for 1D electron systems, which are characterized by the LL fixed point in the renormalization group sense. The standard and exactly solvable LL model is the 1D electron gas with a linear dispersion $[E(k)=rv_F(k-rk_F)]$ around Fermi points $(\pm k_F)$ at each branch $(r=\pm1)$ and with short-ranged forward interaction.[1,2] Using bosonization method and a linear transformation, the LL Hamiltonian can be exactly diagonalized by the two boson operators: charge boson $\rho_r(p)$ and spin boson $\sigma_r(p)$. This fact makes the collective excitation spectra (CDE and SDE) in the Luttinger model very simple: both the charge (CDE) and the spin (SDE) modes are delta function like poles and there is no SPE mode or equivalently, quasiparticle spectral weight, at all. Using the standard Bosonization method, we got for the charge (ρ) and the spin (σ) sector response functions:

$$\chi_\rho(q,\omega)=\frac{2L}{\pi}\frac{K_\rho(q)v_\rho(q)q^2}{(\omega+i\delta)^2-(\omega_q^\rho)^2}, \tag{4}$$

$$\chi_\sigma(q,\omega)=\frac{2L}{\pi}\frac{K_\sigma(q)v_\sigma(q)q^2}{(\omega+i\delta)^2-(\omega_q^\sigma)^2}, \tag{5}$$

where the excitation energy, $\omega_q^{\rho/\sigma}=|q|v_{\rho/\sigma}(q)=|q|v_F/K_{\rho/\sigma}(q)$, and the charge sector Luttinger exponent $K_\rho(q)$ is

$$K_\rho(q)=\left(1+\frac{2V_c(q)}{\pi v_F}\right)^{-1/2}, \tag{6}$$

while $K_\sigma(q)=1$ in the spin sector for the spin-independent Coulomb interaction.

It is clear that the above results are completely spin-charge separated, which is another important feature of the LL model. One should note that there is no spectral weight in $\chi_\rho(q,\omega)$ at $\omega=qv_F$ for any SPE mode (or, for that matter any mode). This shows that the small SPE peak (compared to CDE) in the Fermi-liquid RPA theory is totally absent in the LL theory. Thus any possible explanation within the LL theory for the anomalous low-energy peak in the polarized RRS spectra must arise from some mode (e.g., a multiboson mode or an SSE mode) other than the SPE mode which is completely absent in the LL theory.

We note one other aspect (the spin-charge separation mentioned above) of the LL theory in this context which has created some minor confusion. The spin-charge separation of the LL theory has nothing whatsoever to do with the separate existence of SDE/CDE in the depolarized/polarized RRS spectra. The collective spin- and charge-density excitations are completely distinct excitations in the FL theory as well—they are the poles of the appropriate spin (for SDE) and charge (CDE) density correlation functions of the system which have totally different energies and selection rules (i.e., whether there is a spin flip or not) in any reasonable theory. The reason spin-charge separation is rather complete in the LL theory is because the Luttinger liquid does not have any quasiparticles or single-particle excitations—it has only collective spin and charge excitations which are poles of different correlation functions and are always separate. Indeed, higher dimensional systems, such as 2D and 3D GaAs structures, exhibit qualitatively similar RRS spectra as in the 1D system with the CDE peak (and a weak SPE-like low energy feature) showing up in the polarized spectra and the SDE peak showing up in the (spin-flip) depolarized RRS spectra. These higher dimensional systems are obviously Fermi liquids and have no LL-like intrinsic spin-charge separation while at the same time having distinct CDE and SDE collective modes.

Unlike the formulas for the single-particle Green's function, in which the non-Fermi-liquid-like Luttinger liquid feature arises from the nonperturbative power-law behavior to-

gether with the velocity renormalization, the charge- and spin-density correlation functions (which are two-particle Green's functions) have no such power-law behavior at all. The density correlation functions and the the associated charge-/spin-density excitation collective mode spectra are essentially identical in the LL and the FL-RPA model[3,11] except for the complete absence of any SPE spectral weight in the charge sector in the LL model. The Luttinger liquid effects appear only in the mode velocity renormalization $v_\rho(q)$ and the overall-mode amplitude factors $K_\rho(q)$ in the collective-mode spectra.

The diagrammatic method for the Luttinger liquid theory tells us more about the transition from the Fermi liquid to the Luttinger liquid, because it is physically more transparent than the Bosonization technique, which is more of a formal mathematical tool. Early seminal work by Dzyaloshinkii and Larkin[20] and recent important work of Schultz[21] have shown that this method is equivalent to the Bosonization theory, even though its theoretical structure follows a Fermi-liquid-type conventional many-body theory.

In order to evaluate the irreducible polarizability, we use the Ward identity connecting the Green's function with the vertex function in the following formula:

$$\Gamma_{rs}(p,\nu,q,\omega)=\frac{G_{rs}^{-1}(p,\nu)-G_{rs}^{-1}(p-q,\nu-\omega)}{\omega+i\delta-rqv_F}, \quad (7)$$

where $\Gamma_{rs}(p,\nu,q,\omega)$ is the vertex function of two-particle lines and one interaction line. The Ward identity follows directly from the particle and current conservation in each branch and spin (valid only for forward scattering) coupled with linear dispersion relation. It can be derived by summing the infinite series of vertex diagrams as shown in Fig. 5. Using this vertex expression, one can calculate the exact irreducible polarizability (consider the charge part only)

$$\begin{aligned}\Pi_{0,\rho}(q,\omega)&=-i\sum_{rs}\int\frac{dp}{2\pi}\int\frac{d\nu}{2\pi}G_{rs}(p,\nu)G_{rs}(p-q,\nu-\omega)\\&\quad\times\Gamma_{rs}(p,\nu,q,\omega)\\&=\sum_{rs}\int\frac{dp}{2\pi}\frac{n_{rs}(p-q)-n_{rs}(p)}{\omega+i\delta-rqv_F}\\&=\frac{2q^2v_F/\pi}{(\omega+i\delta)^2-(qv_F)^2}.\end{aligned} \quad (8)$$

Comparing the Fermi-liquid RPA results with the LL results we find that they are identical if we only change the FL-RPA parabolic dispersion to the linear one as in the Luttinger model. Therefore we obtain the striking result that the irreducible polarizability of the linear band dispersion model is exactly the same as the RPA result. In other words, vertex corrections to the irreducible polarizability vanish. This result can also be verified by the topological argument given in Ref. 21, which shows that all the electron-hole loops connecting with more than three interaction lines cancel out.

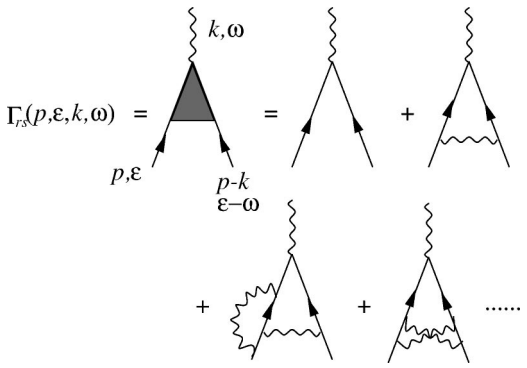

FIG. 5. Diagrammatic representation of the Ward identity for the vertex function Γ_{rs}. The solid lines represent the single-particle Green's function while the wave lines represent the interaction.

Note that the above result is independent of temperature, due to the particle number conservation in the p integral. When the dispersion is linearized as in the LL model, $\mathrm{Im}\Pi_{0,\rho}^{\mathrm{RPA}}(q,\omega)$ itself becomes a delta function at $\omega=qv_F$ rather than a square function, leading to the complete suppression and the disappearance of the SPE mode at $\omega=qv_F$. This makes this diagrammatic result consistent with the Bosonization result, in which there is manifestly no single-particle eigenstate at all in the final spectrum. Both approaches predict the complete absence of an SPE mode in the LL theory.

IV. HUBBARD MODEL

Motivated by the long-standing SPE-feature puzzle discussed in the Introduction, it has been suggested[13,8] that we can interpret the ''SPE'' peak observed in the experimental RRS spectra as the ''singlet spin excitation.[13]'' In other words, the incident photon virtually flips the electron spin and then restores its polarization after the scattering, leaving the electron spin unchanged. Unlike the triplet spin excitation, SDE, which manifests itself in the depolarized RRS spectra, the virtual spin-flip process of SSE may, in principle, contribute to the final spinless scattering matrix element of the polarized Raman scattering spectrum, so one could expect that SSE should be very close to the SPE in energy under the spin-independent Coulomb interaction. That explains why one cannot simply separate these two (SSE and SPE) whether in the experimental measurement or in the theoretical calculation. In the LL theory, there is no SPE, but SSE is, in principle, allowed and may simulate the SPE of the FL-RPA theory. To investigate the role of SSE in more details we could use the 1D Hubbard model on a lattice, which can be mapped to the exactly solvable Luttinger liquid model in the long-wavelength limit. Thus the 1D Hubbard model has no generic SPE properties, and could therefore be useful in the understanding of SSE properties. We therefore study the SSE in the 1D Hubbard model, and investigate whether its spectral weight can be comparable to the CDE as observed in the experiments.

In this paper, we want to study the 1D single band Hubbard model (HM) through the Bethe-ansatz equations and the Lanczos-Gagliano method, which is shown to be in excellent

agreement with the exact diagonalization result. Although HM is a lattice model of short-ranged on-site interaction, unlike the realistic 1D QWR systems which are continuum systems with long-ranged Coulomb interaction, we could still use it as a valid model in qualitatively discussing the problem of the polarized Raman scattering because all 1D interacting systems belong to the LL universality class and generic issues may be addressed in any particular 1D model. We first identify the holon excitation of the Hubbard model to be the CDE, and the triplet spinon to be the SDE in the usual RRS language, by comparing their dispersion relations in the whole spectrum. We then further obtain the finite spectral weights of SSE in the charge-density spectrum and show that the weight of singlet spin-density excitation is still rather low in the HM and *cannot* produce large spectral weights in the polarized RRS scattering spectrum as found in the experiment. Thus our HM results shows that the SPE peak in the polarized RRS experiments is unlikely to be explained by the 1D singlet spin excitation, at least within any nonresonant theory which considers the elementary excitations only in the conduction band.

A. Theory

The simple 1D single band Hubbard model,

$$H=-t\sum_{i,\sigma}\ (c^{\dagger}_{i+1,\sigma}c_{i,\sigma}+\text{H.c.})+U\sum_{i}\ n_{i\uparrow}n_{i\downarrow}\,, \tag{9}$$

where $c_{i,\sigma}$ and $n_{i,\sigma}$ are, respectively, the fermion creation operator and the density operator for site i and spin σ, has been extensively studied. t and U are hopping energy and on-site short range spin-dependent interaction following the usual notation in the literature.[22–24] Note that the Hubbard model is basically a model with a spin-dependent short-range (on-site) interaction U. It has generic LL properties in the long-wavelength limit and for low-lying excitation energy, i.e., no single-particle behavior in the spectral function at Fermi wave vector. The explicitly spin-dependent interaction U in the HM, however, should make the spin singlet state more enhanced in the spectrum, and easier to study. Among the many accurate and useful methods to study the 1D HM, we use the Bethe-ansatz method[22,24] to obtain the ground state and the low-lying excitation state dispersion spectra. It is well known that the Bethe-ansatz wave functions are not particularly useful in calculating correlation functions, and therefore we need an alternative method to obtain the spectral weights of the elementary excitations. We calculate the charge-density and spin-density correlation functions, to be compared respectively with the polarized and depolarized inelastic light scattering spectra, by using the Lanczos-Gagliano method.[25–28] This method (described and discussed below) gives a simple but fast-convergent result for the correlation functions in the lattice model. By comparing the momentum-energy dispersion relations of these two different methods, (i.e., the Bethe-ansatz and the Lanczos-Gagliano method) we can identify each important spectral peak obtained by the Lanczos-Gagliano method to be a certain Bethe-ansatz elementary excitation in the Hubbard model language (holon, triplet spin, or singlet spin excitations, for example) and then estimate their relative weights for comparison. Our results obtained by this technique are consistent with the quantum Monte Carlo calculations[29] where appropriate.

1. Bethe-ansatz equations

It is well known that the 1D Hubbard model can be solved exactly[22,23] by the Bethe-ansatz method. The eigenvalue equation of Eq. (9) is proved to be identical to solving the coupled system of equations (under periodic boundary condition)

$$e^{ik_jL}=\prod_{\alpha=1}^{M}\frac{\sin k_j-\lambda_\alpha+iU/4}{\sin k_j-\lambda_\alpha-iU/4}, \tag{10}$$

$$\prod_{j=1}^{N}\frac{\lambda_\alpha-\sin k_j+iU/4}{\lambda_\alpha-\sin k_j-iU/4}=-\prod_{\beta=1}^{M}\frac{\lambda_\alpha-\lambda_\beta+iU/2}{\lambda_\alpha-\lambda_\beta-iU/2}, \tag{11}$$

where $L(N)$ is the total number of sites (electrons) and M is the number of down-spin electrons ($M\leqslant N/2$). The pseudomomentum $\{k_j\}$ and spin rapidities $\{\lambda_\alpha\}$ are generally complex variables to be solved and related to the physical states of energy E and momentum p by

$$E=-2t\sum_{j=1}^{N}\cos k_j\,, \tag{12}$$

and

$$p=\sum_{j=1}^{N}k_j\,. \tag{13}$$

If the k_j's and λ_α's are all real, the identity of the phases in Eqs. (10) and (11) can be obtained by taking the logarithm. Then we have the following well-known results:

$$Lk_j=2\pi I_j+2\sum_{\alpha=1}^{M}\tan^{-1}\left(\frac{\lambda_\alpha-\sin k_j}{U/4}\right), \tag{14}$$

$$2\sum_{j=1}^{N}\tan^{-1}\left(\frac{\lambda_\alpha-\sin k_j}{U/4}\right)=2\pi J_\alpha+2\sum_{\beta=1}^{M}\tan^{-1}\left(\frac{\lambda_\alpha-\lambda_\beta}{U/2}\right), \tag{15}$$

where the quantum numbers $\{I_j\}$ are all distinct from each other and are integers if M is even and are half-odd integers if M is odd, and are only defined in $|I_j|\leqslant L$. Similarly, the set $\{J_\alpha\}$ are all distinct and are integers if $N-M$ is odd and half-odd integers if $N-M$ is even. The value of $\{J_\alpha\}$ is restricted by $|J_\alpha|<(N-M+1)/2$. Generally, it is not hard to use the Bethe-ansatz equations to solve large size systems. In the thermodynamic limit, $L\to\infty$, one can find the equivalent linear integral equations for the density of k's and λ's on the real axis.[23,30,31] But we will only focus here on the finite-size systems in order to compare the Bethe-ansatz results with the results of the Lanczos-Gagliano method, which is necessarily computationally restricted to small system sizes.

To solve these Bethe-ansatz equations, we first have to define the proper quantum numbers $\{I_j\}$ and $\{J_\alpha\}$, then solve

Eqs. (14) and (15) to get k_j's and λ_α's, and then get the momentum p and the energy E of that state specified by those quantum numbers. Here we present the quantum number structures of the ground state and two low-lying excited state, the "$4k_F$" singlet states, the "$2k_F$" triplet states, and the "$2k_F$" singlet states as named by Schultz.[14] The first two have k's and λ's all real, while the last one has one pair of complex λ's in Eqs. (10) and (11).

Ground state. It is easy to see that the ground state is nondegenerate only if N is of the form $4m+2$ (m is an integer). In the following, we just study the nondegenerate case for simplicity. Considering the essential symmetries, one can write the ground-state quantum number satisfying the above restrictions to be

$$\{I_j\}=\{-(N-1)/2,\ldots,(N-1)/2\},$$
$$\{J_\alpha\}=\{-(N/2-1)/2,\ldots,(N/2-1)/2\}. \tag{16}$$

$4k_F$ singlet state (holon excitation). The first simplest excited states are obtained by removing one of the momentum quantum numbers, $-(N-1)/2+i_0$, in $\{I_j\}$ and adding a "new" one at $(N-1)/2+I_0$ outside the ground-state sequence. All other momentum quantum numbers and spin quantum numbers are kept the same as in the ground-state structure. Therefore the new sequence of $\{I_j\}$ is

$$\{I_j\}=\{-(N-1)/2,\ldots,-(N-1)/2+i_0-1,-(N-1)/2+i_0+1,\ldots,(N-1)/2,(N-1)/2+I_0\}, \tag{17}$$

and the $\{J_\alpha\}$ is the same as the ground state in Eq. (16). Therefore there are two free parameters, i_0 and I_0, for this type of excitations. In this paper, we use (i_0,I_0) to denote this excitation state. According to Schultz,[14] they are named $4k_F$ singlet states due to their energy minimum at $k=4k_F$ in their dispersion spectrum. In the literature, these states are also called "particle-hole excitation" or "holon" excitation.[23] In the rest of this paper, we will call them "holon" excitations for simplicity. (This is related to the CDE of our earlier sections.)

$2k_F$ triplet state (triplet spinon excitation). Next we consider the excitations of the J's with all λ's and k's real. This is possible only if $M<N/2$. The simplest excitations of this type are obtained by considering $M=N/2-1$. The total spin of the system is $S=1$, so we expect this excitation to be related to a triplet spin excitation. The quantum numbers of these states are

$$\{I_j\}=\{-N/2+1,\ldots,-N/2+i_0-1,-N/2+i_0+1,\ldots,N/2,N/2+I_0\},$$
$$J_1=-N/4+\delta_{\alpha_1,1},$$
$$J_\alpha=J_{\alpha-1}+1+\delta_{\alpha,\alpha_1}+\delta_{\alpha,\alpha_2}, \tag{18}$$

where $\alpha=2,\ldots,M$ and $1\leqslant\alpha_1<\alpha_2\leqslant M+2$. Here α_1 and α_2 are the free parameters in the spin quantum number, $\{J_\alpha\}$, and i_0 and I_0 are the two parameters in momentum quantum number $\{I_j\}$. From Eqs. (12)–(15), we can see that i_0 and I_0 shift the total momentum and energy of the spectrum created by the spin excitation in $\{J_\alpha\}$. In the following calculation, we use $(i_0,I_0,\alpha_1,\alpha_2)$ to denote these states in the spectrum. These excitations are called $2k_F$ triplet states because its minimum energy is at $k=2k_F$. In the rest of this paper, we will call them "triplet spinon" for simplicity. (This is related to the SDE of the earlier sections.)

$2k_F$ singlet state (singlet spinon excitation). The third possible elementary excitations are from the complex solutions of Bethe-ansatz equations, Eqs. (10) and (11). Spin singlet states ($M=N/2$ and then $S=0$) are obtained by having one pair of the complex conjugate, $\lambda_\pm=\lambda_R\pm\lambda_I$ with all other k's and λ's real. The new set of Bethe-ansatz equations are obtained to be

$$Lk_j=2\pi I_j+2\sum_{\alpha\neq\alpha_1,\alpha_2}^{M}\tan^{-1}\left(\frac{\lambda_\alpha-\sin k_j}{U/4}\right)+2\left[\tan^{-1}\left(\frac{\lambda_R-\sin k_j}{U/4-\lambda_I}\right)+\tan^{-1}\left(\frac{\lambda_R-\sin k_j}{U/4+\lambda_I}\right)\right], \tag{19}$$

$$2\sum_{j=1}^{N}\tan^{-1}\left(\frac{\lambda_\alpha-\sin k_j}{U/4}\right)=2\pi J_\alpha+2\sum_{\beta\neq\alpha_1,\alpha_2}^{M}\tan^{-1}\left(\frac{\lambda_\alpha-\lambda_\beta}{U/2}\right)+2\left[\tan^{-1}\left(\frac{\lambda_\alpha-\lambda_R}{U/2-\lambda_I}\right)+\tan^{-1}\left(\frac{\lambda_\alpha-\lambda_R}{U/2+\lambda_I}\right)\right], \tag{20}$$

where $j=1,2,\ldots,N$ and $\alpha=1,2,\ldots,M$, but $\alpha\neq\alpha_1$, α_2. The two equations for the complex $\lambda_\pm$ are

$$\frac{1}{2}\sum_{j=1}^{N}\ln\left(\frac{(\lambda_R-\sin k_j)^2+(U/4+\lambda_I)^2}{(\lambda_R-\sin k_j)^2+(U/4-\lambda_I)^2}\right)=\frac{1}{2}\sum_{\beta\neq\alpha_1,\alpha_2}^{M}\ln\left(\frac{(\lambda_R-\lambda_\beta)^2+(U/2+\lambda_I)^2}{(\lambda_R-\lambda_\beta)^2+(U/2-\lambda_I)^2}\right)+\ln\left(\left|\frac{4\lambda_I+U}{4\lambda_I-U}\right|\right), \tag{21}$$

$$\sum_{j=1}^{N}\left[\tan^{-1}\left(\frac{\lambda_R-\sin k_j}{U/4+\lambda_I}\right)+\tan^{-1}\left(\frac{\lambda_R-\sin k_j}{U/4-\lambda_I}\right)\right]=2\pi J+\sum_{\beta\neq\alpha_1,\alpha_2}^{M}\left[\tan^{-1}\left(\frac{\lambda_R-\lambda_\beta}{U/2+\lambda_I}\right)+\tan^{-1}\left(\frac{\lambda_R-\lambda_\beta}{U/2-\lambda_I}\right)\right], \tag{22}$$

where

$$J=\begin{cases}\text{integer} & \begin{cases}\text{if } |\lambda_I|>U/4, \text{ and } N-M \text{ is even}\\ \text{or if } |\lambda_I|<U/4, \text{ and } N-M \text{ is odd}\end{cases}\\ \text{half odd integer} & \text{otherwise.}\end{cases} \tag{23}$$

As for the quantum number, $\{I_j\}$ and $\{J_\alpha\}$, in the singlet states, we choose them to be the same as the ground state, Eq. (16), except for the two free ''holes'' at J_{α_1} and J_{α_2}, whose related spin quantum numbers, λ_{α_1} and λ_{α_2} are replaced by the pair of complex conjugate, $\lambda_\pm = \lambda_R \pm \lambda_I$. Equations (19)–(22) are usually too complex to give a nontrivial solution because the usual numerical iteration method will converge to the trivial $\lambda_I = 0$ solution. But one can simplify these equations by taking $\lambda_I = U/4$ and one k_j satisfying $\sin k_j = \lambda_R$, so that Eq. (21) could be neglected, and all the terms containing $\tan^{-1}[(\lambda_R - \sin k_j)/(U/4 - \lambda_I)]$ in Eq. (22) contribute a phase $\pm\pi$. The phase number J is set to make the total phase shift (including those from $\tan^{-1}[(\lambda_R - \sin k_j)/(U/4 - \lambda_I)]$) to be zero in the calculation.

The spin singlet excitations have a dispersion similar to the triplet ones. Here we could use (α_1, α_2) as the quantum number to define these states. In the finite-size system with repulsive interaction U the singlet states have higher energy than the triplet ones, but they will become degenerate in energy as we go to the thermodynamic limit ($L \to \infty$, and $\langle n \rangle = \text{const}$). In the experiment, the spin triplet excitations (i.e., SDE) are observed in the depolarized RRS spectra where a net spin flip occurs, while the singlet states are observed in the polarized spectra, which involve no net spin flip.

As mentioned in the beginning of this section, the Bethe-ansatz method does not, in general, provide the spectral weights for their solutions. Therefore the three elementary excitations above may not be equally important from the experimental point of view, i.e., they may carry very different spectral weights (and some may even be unobservable in the experimental spectra). All we know from the Bethe-ansatz solutions are the existence and the dispersion of these excitations but *not* their spectral weights. We also know that these are allowed solutions of the HM just as the SPE is an allowed solution of the FL-RPA model (but *not* the LL model). Comparing the mode spectral weights calculated by Lanczos-Gagliano method we discuss next, we calculate the relative spectral weights of these solutions and then study their interaction dependence.

2. Lanczos-Gagliano method

In this paper Lanczos-Gagliano method means the combination of two important techniques in the lattice model. The standard Lanczos method is to construct an $L \times L$ matrix representation for the tridiagonal Hamiltonian, like Eq. (9), and then directly diagonalize it to get the eigenvalues E_n and eigenfunctions Φ_n, which could be used to do further calculations, such as obtaining spectral weights. But since only ground state energy and wave function are needed in calculating the correlation function by using Gagliano's method (see below), we use a simpler but more efficient way, the modified Lanczos method, to calculate the ground-state energy and wave function. This method has been analyzed and discussed in detail in Refs. 25–28 and we refer the reader to the existing literature[17,25–28] for details on the Lanczos-Gagliano method.

B. Results and discussion

We study the 1D Hubbard chain with three different densities, $\langle n \rangle = N/L = 1/3$ for 6 electrons in 18 sites, $\langle n \rangle = 1/2$ for 6 electrons in 12 sites, and $\langle n \rangle = 5/6$ for 10 electrons in 12 sites. (Note that the usual filling factor of the system is $\langle n \rangle/2$ since our definition of density does not include spin.) The size of the Hubbard chain is dictated here entirely by computer memory restrictions in calculating the correlation function via the Lanczos-Gagliano method. We keep the electron number to be $4m+2$ with m an integer in order to have a nondegenerate and zero-momentum ground state under the periodic boundary condition. Throughout our calculations, we set the broadening factor to be $0.01t$ [where t is the nearest-neighbor hopping amplitude in Eq. (9)] and use the modified Lanczos method to calculate the ground-state energy iterationally until convergence to within less than 0.1% in the ground-state energy is reached. We also truncate the infinite continuous fraction at 25–27th order terms, which gives us good convergent results in the calculation.

In the following, we will first discuss the results related to the polarized spectrum, which involves no net spin-flip in the system, by using the two methods mentioned above at a fixed interaction strength, $U/t = 3$. Then we consider the depolarized spectrum under the same conditions. Finally we discuss their interaction U dependence by varying U/t in our calculations. In the discussion below the terms ''resonance'' or ''resonance peaks'' refer to the Lanczos-Gagliano calculations.

1. Polarized spectrum analysis

We compare the dispersion of the charge-density excitation with the dispersions of the $4k_F$ singlet states (holon) and the $2k_F$ singlet states (singlet spinon) given by the solutions of the Bethe-ansatz equations, because these two are the low-lying elementary spinless ($S=0$) excitations of the 1D Hubbard model and as such should correspond to the polarized spectrum. We will also study their relative spectral weights. Both lower density ($\langle n \rangle = 1/3$) and higher density ($\langle n \rangle = 5/6$) results are shown together (Figs. 6–9) for further discussion.

In Fig. 6(a), we show the spectral dispersion obtained by the poles of the imaginary part of the charge density correlation function. The doping density is $\langle n \rangle = 1/3$ for 6 electrons in 18 sites in the 1D Hubbard chain with periodic boundary conditions. The center of each open diamond represents the position of the pole, and its area is proportional to the spectral weight of that excitation. In the same figure, the dispersions of the holon (star) and singlet spinon (open square) excitations given by the solutions of Bethe-ansatz equations are also shown for comparison. Several features could be noted from Fig. 6: (i) the excitation peaks of the charge-density correlation function have a linear dispersion in the long-wavelength limit ($q \ll k_F = \pi/6$) and its slope gives the velocity of charge density excitation of 1D Hubbard model. (ii) The resonance peaks form a wing up to the large momentum region (i.e., low-energy excitations correspond to the low momentum and high ones to high momentum), with a maximum energy $\omega = 4t$ at $q = \pi$. (iii) The sizes

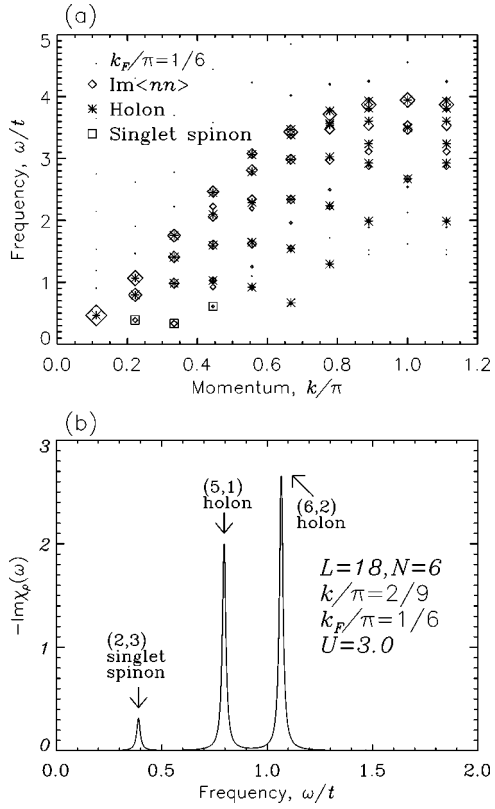

FIG. 6. (a) Energy-momentum dispersion relation and (b) the spectrum of charge-density correlation function for 6 electrons in 18 sites. The area of each diamond (square) in (a) is proportional to the spectral weight of each charge (spin) excitation peak. The numbers above the holon and singlet spinon peaks in (b) are the quantum numbers defined in Sec. IV A 1 from the Bethe-ansatz equations.

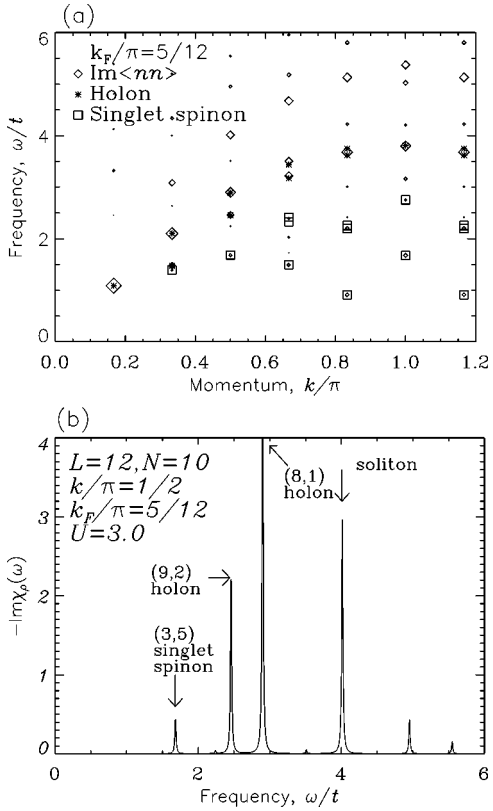

FIG. 7. Same as Fig. 6, but for 10 electrons in 12 sites. One can see that the double occupancy of electrons will give higher-energy excitations in this high-density system. Even the singlet spinon excitations span in a larger area in the whole momentum range in (a), their spectral weights are still smaller than the holons and solitons (double occupancy excitations).

of the diamonds, which represent their spectral weights, show that the peaks at higher energy generally have greater spectral weights than the ones at lower energies at the same momentum (i.e., spectral weights are greater for peaks at higher energies). Therefore one could see by eye a sinelike curve at the upper edge of the resonance wing with a maximum at $\omega=4t$, and this observation is consistent with the results from quantum Monte Carlo simulations on larger system.[29] (iv) There are no excitation states for singlet spinons at small $q=\pi/9$. This implies that the singlet spinon of the 1D Hubbard model is not allowed for momentum smaller than $2\times 2\pi/L$, where $2\pi/L$ is the momentum scale of this finite-size (L) system. This follows from the fact that the singlet state must be excited by a pair of complex conjugate $\lambda_\pm$ in Eqs. (10) and (11), which is at least a two-particle excitation, so that the minimum momentum required is $2\times 2\pi/L$. (v) One interesting feature is that there are clearly two energy minima at $q=2k_F=\pi/3$ and $q=4k_F=2\pi/3$ in the spectrum. Comparing these resonance peaks with the solutions given by Bethe-ansatz equations, we find that the holon excitations cover almost exactly the same region including the energy minimum at $4k_F$ except for the lower-lying peaks around $2k_F$, where the singlet spinon just matches those peaks. In other words, we could reasonably claim that the most dominant features of the resonance peaks given by the charge-density correlation function arise from a combination of holon and singlet spinon excitations in the 1D Hubbard model. This result could not be trivially obtained either by solving Bethe-ansatz equations or by calculating the charge-density correlation function alone, as mentioned in the introduction—one must combine the two techniques to come to this conclusion. Other spin singlet excitations given by the solutions of Bethe-ansatz equations [for example, two pairs of complex λ's in Eqs. (10) and (11)], carry very small spectral weights because no other significant resonance peaks are found in this dispersion spectra, except for some trivial ones. In the thermodynamic limit, we expect that only the $4k_F$ holon and $2k_F$ singlet spinon will have finite spectral weights and could be interpreted as the ''charge-density excitation'' and ''single-particle excitation'' in the RRS spectra respectively when comparing with the experiments[4] as we mentioned in the earlier sections. We discuss this issue further later in this paper.

In Fig. 6(b), we show the imaginary part of the charge-density correlation function of the same system at $q=2\pi/9$. It shows that singlet spinons have a relatively small, but non-negligible weight, compared with the weight of the dominant holon excitations. Their relative spectral weight ratio (singlet spinon/holon) is less than 0.1. Similar results are also obtained in the systems of 6 electrons in 12 sites,

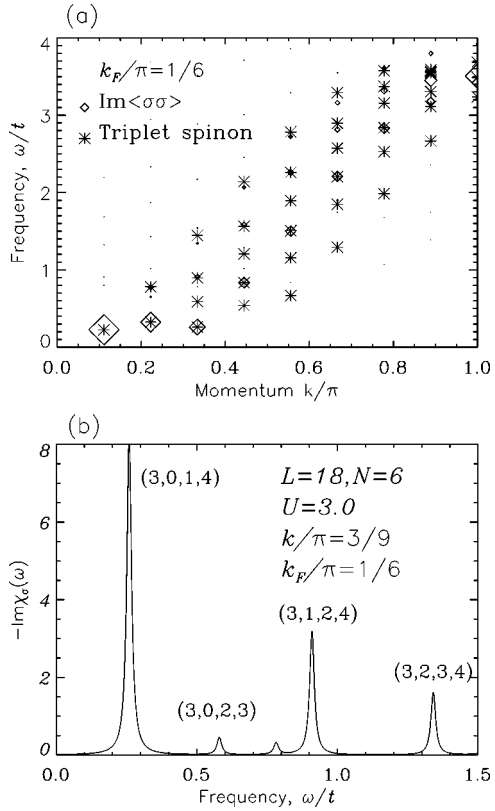

FIG. 8. (a) Energy-momentum dispersion relation and (b) the spectrum of the spin-correlation function for 6 electrons in 18 sites.

$\langle n\rangle=1/2$, which are not shown in this paper.

In Fig. 7(a), we show the dispersion of the resonant poles of the charge-density correlation function of 10 electrons in 12 sites ($\langle n\rangle=5/6$). Here the holon excitations form a more narrow wing than in the lower density system, but the basic shape of the dominant curve is almost the same. Below this curve, the singlet spinon occupies almost the whole resonance region. Since $4k_F=5\pi/3$ in this high-density system, we cannot see the $4k_F$ energy minimum in this figure (actually, the gap of this energy minimum is very large in this finite system, but will go to zero in the thermodynamic limit[14]). But one could still see the energy minimum of the singlet spinon at $2k_F=5\pi/6\sim 0.833\pi$ in Fig. 7(a). There is a notable feature in these results at energies above the holon

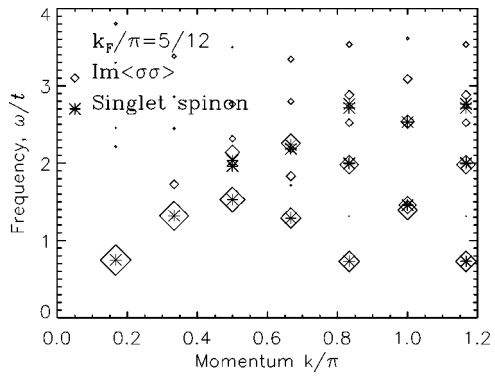

FIG. 9. Same as Fig. 8(a), but for 10 electrons in 12 sites.

excitations: there are some additional states, having an energy gap equal to $U(=3t)$ and a maximum energy greater than $4t$ at $q=\pi$ in this high-density situation. These states (solitons) must arise from the double occupancy of the electrons in the Hubbard model, which consequently explains their high-energy status. The quantum Monte Carlo method, to the best of our knowledge, does not provide any information about these high-energy double occupancy states at the same density $n=5/6$ in the literature.[29] From the Bethe-ansatz equations point of view, however, these states should be obtained by taking the complex momentum k_j solutions in Eqs. (10) and (11),[30] whether in the high- or the low-density system. Once again, we see the importance of studying the spectral weights of the Bethe-ansatz solutions by comparing them to the correlation function results so that one could tell the most realistic and physically meaningful states. Just having the solutions, without much idea about their spectral weights, is not useful in determining the experimental and/or physical relevance of the particular excitations. Therefore, as shown in Fig. 7(b), the three most important contributions to the charge-density correlator arise from singlet spinon, holon, and soliton excitations (double occupancy excitations), from lower energy to higher energy regime, respectively, in the 1D Hubbard chain. Their relative spectral weights show that the singlet spinon has the smallest weight, and it could be shown that there are *no* gapless holon and singlet spinon excitations in the half filling ($\langle n\rangle=1$) 1D Hubbard model systems, where the soliton (double occupancy excitations) and other higher energy states dominate the excitation spectrum.

2. Depolarized spectrum analysis

In Fig. 8(a), we show the resonance dispersion spectrum of the spin-density correlation function, $\langle\sigma\sigma\rangle$, of the low-density system (6 electrons in 18 sites). The triplet spinon excitation spectrum given by the solutions of Bethe-ansatz equations is also presented for comparison. Several features are found: (i) in the long-wavelength limit, the resonant poles have a linear dispersion, whose slope gives the velocity of the spin-density excitation. One could easily see that this velocity is always smaller than the velocity of the charge-density excitations at the same density. This is consistent with result of previous work.[14] (ii) The resonance poles form a wing up to the large momentum region ($q\sim\pi$), whose maximum excitation energy is below $4t$. (iii) Unlike the results for the charge-density correlation function in Fig. 8(a), the most dominant poles are located in the lower energy part of the resonance wing, which correspond to the triplet state without any excitations in $\{I_j\}$, and therefore is related to the lowest energy ones in our calculation. (iv) The resonance spectrum has an energy minimum at $2k_F$. Compared to the triplet solutions of Bethe-ansatz equations, the triplet spinon excitation spectrum has only three peaks matching the resonance poles of the largest spectral weight at their momentum values ($q=\pi/9$, $2\pi/9$, and $3\pi/9$), and the other three match the poles of relatively much *weaker* states [not visible in Fig. 8(a), but distinguishable in the absorption spectrum shown in Fig. 8(b)]. This result demonstrates that the spectral weights of elementary excitations could be very different even if they

result from the same type of the Bethe-ansatz solution. Figure 9 shows the dispersion relation of the spin-density correlator of the large density system ($\langle n\rangle = 5/6$) and the corresponding triplet spinon excitations by the Bethe-ansatz solutions are also shown.

3. Interaction dependence

In this section, focusing on the lower density system ($L=18$ and $N=6$) and a fixed momentum ($k=2\pi/9$), we study the mode dispersion and spectral weight of these excitations in a range of finite interaction ($U/t \leqslant 10$) to obtain the interaction dependence of the excitation spectra. First, we study the polarized spectrum given by the imaginary part of the charge-density correlation function, $\langle \rho\rho \rangle$ [shown in Fig. 10(a)]. Then we compare the energy of the resonance peaks in the series of spectra with the Bethe-ansatz results [Fig. 10(b)], and discuss the interaction dependence of the mode velocity [Fig. 10(c)]. Finally we discuss the interaction dependence of the spectral weight for each elementary excitation [Fig. 11].

In Fig. 10(a), there are basically three peaks in the typical structure of the polarized spectrum, and we can identify them as the singlet spinon, the second and the first holon excitation (from lower to higher energy) by explicitly comparing with the energy given by the Bethe-ansatz solution in Fig. 6(a). Using the notation introduced in Sec. IV A 1, the singlet spinon is the state (2,3), while the holon I and II states are (6,2) and (5,1), respectively. Several interesting features can be found in Fig. 10(a): (i) in the noninteracting ($U=0$) case, there are only two equal weight poles, which could be understood as the two single particle (electron and hole) excitations around Fermi surface, $k=k_F$. (ii) When finite interaction is turned on, there is an additional excitation. According to the comparison of dispersion relations, both the new peak and the higher energy peak should be interpreted as holon excitations (called holon II and holon I, respectively, corresponding to different $\{I_j\}$'s). (iii) The singlet spinon excitation [shown in Fig. 10(a)] has a rapidly decreasing spectral weight with increasing interaction, and disappears totally as $U/t > 5.0$. (iv) The two holon excitations shift to higher energy as U increases, and maintain almost the same spectral weight except one more peak appears as $U/t \geqslant 8.0$ [see Fig. 10(a)]. Above $U/t=8.0$, the appearance of the new small peak affects both the spectral weight and excitation energy of the holon II excitations [see Figs. 10(b) and 11(a)]. There are basically two possible interpretations for this result. One is that this peak does not represent real excitations, but may be arising spuriously from the inaccuracy of the finite truncated series or finite iteration used in the Lanczos-Gagliano method in the large U range. Another possible reason is that it may arise from the higher energy excitation states of unknown origin, which are also obtainable from the Bethe-ansatz solutions, but whose strength is visible only when the interaction strength is large enough. We will not discuss this anomalous peak any further in this paper since this falls outside the scope of our main interest.

In Fig. 10(c), we plot the excitation velocity, which is defined to be

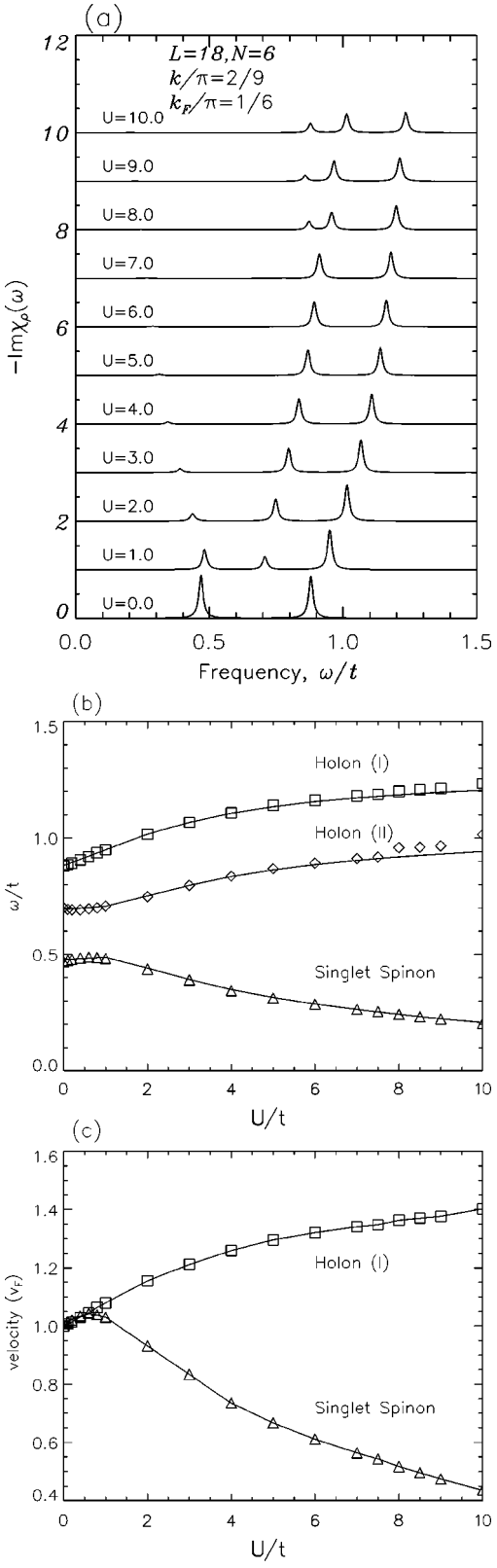

FIG. 10. (a) The calculated polarized spectra with various interaction strengths for $\langle n\rangle = 6/18 = 1/3$, at $k=2\pi/9$, and (b) the excitation energies of the three elementary exciations in various U/t, compared with the Bethe-ansatz results (solid lines). (c) The velocities of holon and singlet spinon with respect to the Fermi velocity v_F as a function of U/t.

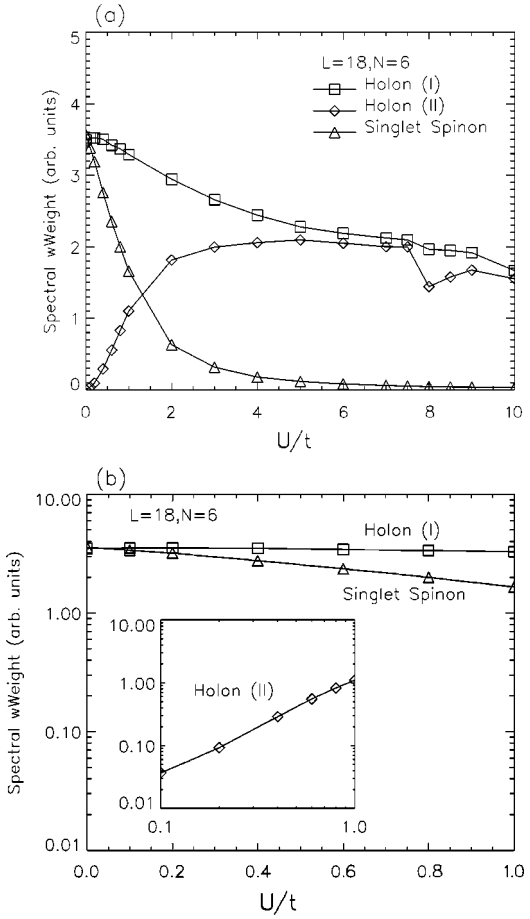

FIG. 11. The spectral weights of the three excitations in the polarized spectrum as a function of the interaction strength U/t in (a) linear scale from $U/t=0$ to $U/t=10$, and (b) linear-log scale for small U ($U/t\leqslant 1.0$). The momentum $k=2\pi/9$ is the same as in Fig. 6. The inset of (b) is the log-log plot for the holon II excitation. We can see that the holon II excitation increases as a power law in its strength as U increases, showing a possible Luttinger liquid behavior in the weakly interacting system (see text).

$$v\equiv\left.\frac{\Delta E(q)}{\Delta q}\right|_{q\to 0^+}, \tag{24}$$

as a function of interaction strength. We find that when the interaction is weak ($U/t\leqslant 1$), the two (holon and singlet spinon) excitations are almost degenerate, while their relative spectral weights change a lot [see Fig. 11(a)] as a function of U/t. When U/t increases, the holon has greater excitation energy and hence velocity, but the velocity of the singlet spinon decreases fast. This result holds even in the thermodynamic limit.

In Fig. 10(b), we see more clearly that the energies of the three elementary excitations are only weakly dependent on the interaction for small U, but strongly dependent on U for large U. In Fig. 11(b), we have a logarithmic scale in the spectral weight dependence with respect to the interaction in small U/t range ($U/t<1.0$). By calculating the slope of these data, we find that the spectral weight of holon I, $S_{\text{holon I}}$, is almost a constant in the smaller interaction range ($U<0.5t$), and then weakly decreases for higher U. However, the spectral weight of holon II has a stronger power-law behavior, $S_{\text{holon II}}\propto U^{1.635}$. Thus the two holon excitations differ a great deal in their interaction dependence of their respective spectral weights.

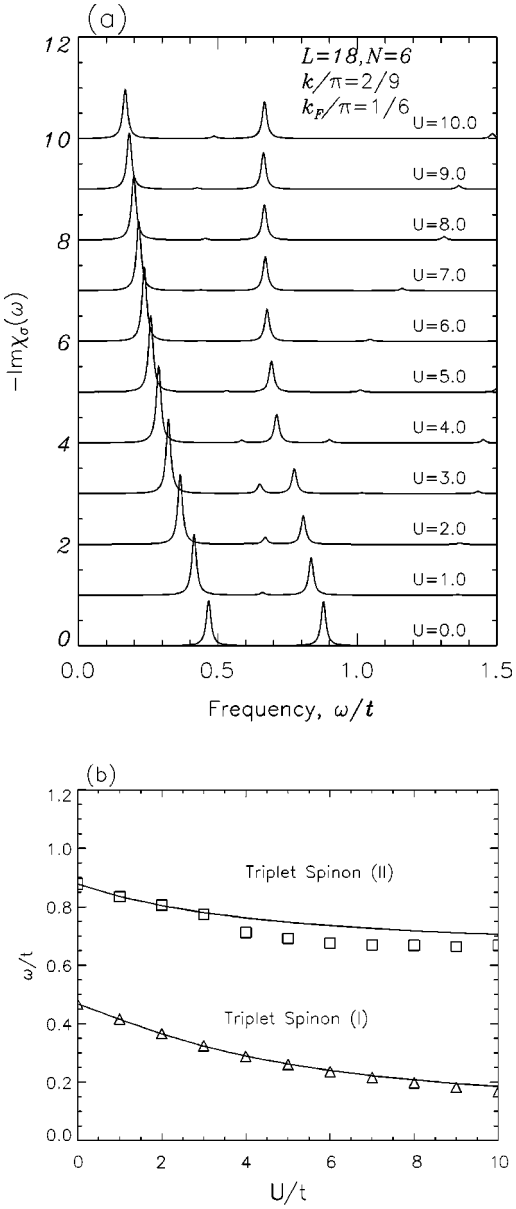

FIG. 12. (a) The calculated depolarized spectra with various interaction strengths of the low-density system, $\langle n\rangle=6/18=1/3$, at momentum $k=2\pi/9$, and (b) the excitation energies of the two elementary excitations (triplet spinon I and II) with respect to the interaction strength, U/t, compared with the Bethe-ansatz result (solid lines).

In Fig. 12(a) we show the calculated depolarized spectra by taking the imaginary part of spin density correlation function, $\langle\sigma\sigma\rangle$ for various interaction strengths. In the noninteracting case, the spectrum is the same as the polarized one in Fig. 6(a) due to spin rotational symmetry. But with increasing interaction strength both triplet spinon peaks move to lower energy in contrast to the polarized spectra. Compared with the Bethe-ansatz results in Fig. 12(b), the lower/higher

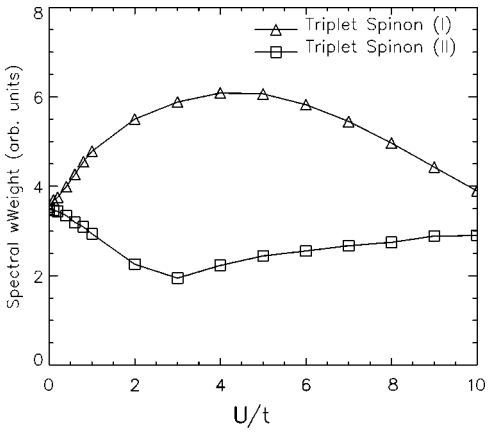

FIG. 13. The spectral weights of the triplet spinon excitations as a function of interaction U/t in linear scale from $U/t=0$ to $U/t=10$. We consider the same system and momentum as in Fig. 12.

energy peak, triplet spinon I/II, is the state denoted by (6,0,1,3)/(6,1,2,3). The excitation energy of the triplet spinon we obtain by the Lanczos-Gagliano method agrees well with the Bethe-ansatz result in general except that the energy of the triplet spinon II does not seem to agree well when the interaction is larger than $U/t=3$. From the result in Fig. 12(a), we can see that this may be due to the appearance of another excitation peak in the Lanczos-Gagliano spectra, which is not represented in our Bethe-ansatz solutions. Based on these results we conclude that the triplet spinon excitations are likely to be the dominant contributions in the depolarized spectra. In Fig. 13, we show the interaction dependence of the spectral weights of the two triplet spinon excitations. The triplet spinon I(II) has a maximum(minimum) spectral weight at some finite interaction, $U/t=3\sim4$, and the interaction dependence of the spectral weight is nontrivial. This result demonstrates the importance of the intermediate interaction strength of the 1D Hubbard model.

C. Discussion

We systematically study the elementary excitations of 1D Hubbard model by combining the techniques of the exact Bethe-ansatz equations for the mode dispersion and the Lanczos-Gagliano method based spectral weight calculation of the correlation functions. Three types of elementary excitations, holon, singlet spinon, and triplet spinon excitations, are studied at zero temperature and different densities ($\langle n\rangle=5/6$, 1/2 and 1/3) and different interaction strength U. We first compare the energy-momentum dispersion relations of these excitations obtained by both methods and then study the mode spectral weights in different situations. The comparison between Bethe-ansatz solutions and resonance peaks of the Lanczos-Gagliano correlation function gives us some important results: (i) the holon and the singlet spinon excitation states show up together in the charge-density correlation spectra. Holon states have higher energy with an energy minimum at $k=4k_F$ while the singlet spinons lie in the lower energy region with an energy minimum at $k=2k_F$. There are *no* other states of prominent spectral weights except the gapped double occupancy (soliton) states near half filling. This result connects the theoretical calculation of the 1D Hubbard model with observable physical quantities — in particular, these are the only two modes which are likely to show up in the polarized Raman-scattering experiment probing the charge-density excitation spectra. Another implication of this result is that one can interpret the Bethe-ansatz quantum numbers, $\{I_j\}$ and $\{J_\alpha\}$, as the ones of collective excitations. But our spectral weight analysis shows that most of the Bethe ansatz solutions for the 1D Hubbard chain do not have any observable contributions to the real physical quantities because they carry essentially no spectral weights. (ii) The excitation holon II has a power-law behavior in its spectral weight with respect to the interaction strength in the small U/t region, while the holon I has almost interaction-independent spectral weight (here the holon I/II could be generalized to represent the $4k_F$ singlet excitations having holes in the edge/middle of the charge quantum number $\{I_j\}$). An interesting problem for further research is to obtain an analytic formula for the exponent of the holon II excitation. This will relate to the small interaction expansion of Bethe-ansatz equations and wave functions, which have not yet been explored much in the literature. When the interaction strength increases, on the other hand, the spectral weights of these two holons become equal as shown in Fig. 10(a). (iii) As for the singlet spinons, we find that their spectral weights decrease to zero very fast (exponentially) as U increases. This could be understood from the fact that the on-site repulsive interaction U prevents the formation of the symmetric electron orbital wave functions, which must accompany the antisymmetric spin singlet wave function, thus suppressing the singlet spectral weight for large U. (iv) From the imaginary part of the spin-density correlation functions we find that the triplet spinon is the only low-energy spin excitation in the long-wavelength limit. There is *no* other excitation of important spectral weights in this region. (v) The spectral weight study shows that among many triplet spinon excitation states, only those with some some special quantum numbers could possibly have relatively greater weights at a given momentum [see Fig. 8(a) and the text related to that] for finite interaction strength U/t. Others have very small or trivial weights, which are not physically significant. (vi) Finally the interaction dependence of the spectral weights of the triplet spinon I and II differs very much in the intermediate interaction range, but becomes similar in magnitude in both the weakly interacting and the strongly interacting situations. This shows the subtle complications in interpreting various excitation modes in the 1D Hubbard model for intermediate interaction strength (say $U/t\sim3$). Further research is needed to provide a more complete understanding of this intermediate interaction region, and our results should be considered a preliminary investigation.

V. CONCLUSION

In summary, we systematically calculate the charge-density (polarized spectra) and the spin-density correlation (depolarized spectra) functions of one-dimensional systems in three different models: Fermi liquid model, Luttinger liq-

uid model, and Hubbard model. In the polarized spectra, we find that the FL model shows a strong collective charge-density excitation at plasmon energy and a relatively weak single-particle excitation at $\omega = qv_F$, while the LL model shows one bosonic (plasmon/CDE) excitation only. Comparing the plasmon excitation energy of FL model and the bosonic excitation of LL model we find these two excitations are identical, and the small SPE peak in FL model arises from the finite curvature effect of electron energy dispersion at the Fermi point. In the Hubbard model, however, two excitations, holons and singlet spinons, show up together in the polarized spectra. We show that the holon excitations are actually the CDE in FL model or the bosonic excitation in LL model, while the singlet spinons in the HM arise from the spin degree of freedom and finite dispersion curvature at Fermi point. If we compare the spectral weights of the lower energy excitations (SPE of FL model/no peak in LL model/ singlet spinons in Hubbard model) and the weights of the higher energy excitations (CDE in FL model/boson peak in LL model/holons in Hubbard model), we find that the higher energy excitations always have (much) larger spectral weight than the lower energy ones in all models. This shows that the equal weight two-peak structure observed in the experiments[4] could not be explained by the *nonresonant* Raman scattering mechanism, no matter how one interprets the lower energy excitations to be SPE or SSE. Recent theoretical work[7–9] on *resonant* Raman scattering spectroscopy indicates that the low-energy SPE feature may be a purely band-structure effect arising from the participation of the valence band in the resonant scattering process. This also explains why this anomalous peak shows up in all dimensions in experiments and not just in 1D. In the depolarized spectra, however, only one spin excitation (the SDE or the spin triplet excitation) is observed in these three models. The vertex correction of the FL model will in general reduce the SDE energy compared with the SPE energy, and separate the SDE from the SPE. In the intermediate interaction region, the two triplet spinons in the Hubbard model have very different spectral weight behavior, showing very interesting interaction effects which need to be studied in more details in the future.

ACKNOWLEDGMENTS

The authors are very grateful to the late Professor Heinz Schulz for helpful correspondence on the one-dimensional Hubbard model. This work was supported by the US-ONR and US-ARO.

[1] F.D.M. Haldane, J. Phys. C **14**, 2585 (1981).
[2] J. Voit, Rep. Prog. Phys. **58**, 977 (1995).
[3] S. Das Sarma and E.H. Hwang, Phys. Rev. B **54**, 1936 (1996).
[4] A.R. Goñi, A. Pinczuk, J.S. Weiner, J.M. Calleja, B.S. Dennis, L.N. Pfeiffer, and K.W. West, Phys. Rev. Lett. **67**, 3298 (1991).
[5] C. Schüller, G. Biese, K. Keller, C. Steinebach, and D. Heitmann, Phys. Rev. B **54**, R17 304 (1996).
[6] B. Jusserand, M.N. Vijayaraghavan, F. Laruelle, A. Cavanna, and B. Etienne, Phys. Rev. Lett. **85**, 5400 (2000).
[7] S. Das Sarma and D.W. Wang, Phys. Rev. Lett. **83**, 816 (1999).
[8] M. Sassetti and B. Kramer, Phys. Rev. Lett. **80**, 1485 (1998).
[9] D.W. Wang, A.J. Millis, and S. Das Sarma, Phys. Rev. Lett. **85**, 4570 (2000).
[10] J.K. Jain and P.B. Allen, Phys. Rev. Lett. **54**, 947 (1985); S. Das Sarma and P. Tamborenia, *ibid.* **73**, 1971 (1994).
[11] Q.P. Li and S. Das Sarma, Phys. Rev. B **43**, 11 768 (1991); Q.P. Li, S. Das Sarma, and R. Joynt, *ibid.* **45**, 13 713 (1992).
[12] E.H. Hwang and S. Das Sarma, Phys. Rev. B **50**, 17 267 (1994).
[13] H.J. Schulz, Phys. Rev. Lett. **71**, 1864 (1993).
[14] H. J. Schulz, in *Correlated Electron Systems*, edited by V. J. Emery (World Scientific, Singapore, 1993).
[15] G.D. Manhan, *Many Particle Physics* (Plenum, New York, 1990); D. Pines and P. Nozieres, *The Theory of Quantum Liquids* (Addison-Wesley, Reading, MA, 1989).
[16] J. Hubbard, Proc. R. Soc. London, Ser. A **243**, 336 (1957).
[17] D.W. Wang and S. Das Sarma, cond-mat/0101061 (unpublished). This preprint gives much of the underlying theoretical details and equations not explicitly shown in this paper.
[18] I.K. Marmorkos and S. Das Sarma, Phys. Rev. B **45**, 13 396 (1992).
[19] P.A. Wolff, Phys. Rev. **171**, 436 (1968); F.A. Blum, Phys. Rev. B **1**, 1125 (1970).
[20] I.E. Dzyaloshinkii and A.I. Larkin, Sov. Phys. JETP **38**, 202 (1974).
[21] K. Penc and J. Sólyom, Phys. Rev. B **44**, 12 690 (1991).
[22] E.H. Lieb and F.Y. Wu, Phys. Rev. Lett. **20**, 1445 (1968).
[23] C.F. Coll, Phys. Rev. B **9**, 2150 (1974).
[24] C.N. Yang, Phys. Rev. Lett. **19**, 1312 (1967).
[25] E.R. Gagliono, E. Dagotto, and A. Moreo, Phys. Rev. B **34**, 1677 (1986).
[26] E.R. Gagliono and C.A. Balseiro, Phys. Rev. Lett. **59**, 2999 (1987).
[27] E.R. Gagliono and C.A. Balseiro, Phys. Rev. B **38**, 11 766 (1988).
[28] E.R. Gagliono and C.A. Balseiro, Phys. Rev. Lett. **62**, 1154 (1989).
[29] R. Preuss, A. Muramatsu, W. von der Linden, F.F. Assaad, and W. Hanke, Phys. Rev. Lett. **73**, 732 (1994); M.G. Zacher, E. Arrigoni, W. Hanke, and J.R. Schrieffer, Phys. Rev. B **57**, 6370 (1998).
[30] F. Woynarovich, J. Phys. C **15**, 85 (1982); **15**, 97 (1982).
[31] T.C. Choy and W. Young, J. Phys. C **15**, 521 (1982).